Optics Communications 284 (2011) 2061–2064

Contents lists available at ScienceDirect

Optics Communications

journal homepage: www.elsevier.com/locate/optcom

Double-resonance plasmon and polarization effects in a SERS fiber sensor with a grid nanostructure

Ming Tian [a], Ping Lu [a,*], Axel Schülzgen [b], Nasser Peyghambarian [b], Deming Liu [a]

[a] College of Optoelectronic Science and Engineering, Huazhong University of Science and Technology, Wuhan, Hubei, 430074, China
[b] College of Optical Sciences, The University of Arizona, Tucson, AZ 85721, USA

ARTICLE INFO

Article history:
Received 25 August 2010
Received in revised form 1 November 2010
Accepted 10 December 2010
Available online 29 December 2010

Keywords:
Localized surface plasmon
Surface enhanced Raman scattering
Grid nanostructure
Polarization

ABSTRACT

We presented a systematic study of surface enhanced Raman scattering (SERS) fiber sensor with a grid nanostructure. The plasmonic resonance peak is stable when measuring gas and double-resonance plasmon can be effectively excited; meanwhile local electric field can be strongly enhanced with the metal coated nanostructured fiber facet. Studies on the influence of polarization effects, the plasmon resonance wavelength shift is relatively small in our structure.

© 2011 Elsevier B.V. All rights reserved.

1. Introduction

One of the advantages of using Raman spectroscopy is its capability of providing highly resolved vibrational information and that it does not suffer from rapid photobleaching. However, Raman scattering is an extremely inefficient process. To improve the detection sensitivity, signal amplification can be obtained by exploiting the surface enhanced Raman effect. SERS (surface enhanced Raman scattering) [1–4] is a very powerful Raman technique, being able to provide a spectrum intensity enhancement by orders of magnitude. The phenomenon occurs when adsorbing the target molecules onto nanometersized roughened metal (Ag, Au, Cu, and some others) surface, or in colloids of metals. Nanoscale surface roughness supports the electromagnetic resonance, which is the dominant mechanism of enhancement. These electromagnetic resonances can increase the scattered intensity by 10^4. A second mechanism, referred to as the chemical mechanism, is connected to the creation of new electronic states due to adsorbate–substrate bonding interactions. It is estimated that the chemical mechanism can also greatly enhance the scattering cross section [5].

Based on the above principles, there has been a lot of interest in developing the SERS sensors based on optical fiber. Examples include angled tip fiber sensor, D-shaped fiber sensor, nanorod array fiber sensor, and hollow core photonic crystal fiber [6–11]. Using optical fibers as a SERS platform provides a number of advantages. First, optical alignment is easy and the confinement of light to the fiber core is assured once the light is coupled into the fiber. Second, the detection location is well-defined and easy to control. Third, there are a number of ways to make the SERS active surfaces on the fiber tip, including UV lithography, nanosphere lithography, e-beam lithography, and focused ion beam (FIB) [12].

Of course, there has been particular interest in the use of patterned structures on the distal end of SERS fiber sensors [13–15]. But, they have some disadvantages, such as the resonance wavelength of the nanostructures is not consistent with the pump wavelength and, therefore, the pump light may not couple efficiently to intrinsic plasmon excitations of the nanostructures.

In order to solve these problems, we presented a novel design of a SERS fiber sensor with a grid nanostructure that could be fabricated on the distal end of an optical fiber (GNF). Electromagnetic fields and local field enhancement were studied theoretically using a three-dimensional finite-difference time-domain (FDTD) algorithm. We have studied the transmission spectrum in different thicknesses of the metal film. We demonstrate that in the proposed grid structure surface plasmon (SP) [16] excitation is very effective and strong local field enhancement can be achieved.

2. Structure and simulation

The basic geometry of the grid nanostructure on the distal end of the optical fiber is shown in Fig. 1, which has an outer diameter of 125 μm and a rectangular core with a dimension of 6 μm by 6 μm and there exists a 30 by 30 element array, constructed with alternative high/low index glasses inside the square core. In the production of the grid

* Corresponding author.
E-mail address: pluriver@163.com (P. Lu).

0030-4018/$ – see front matter © 2011 Elsevier B.V. All rights reserved.
doi:10.1016/j.optcom.2010.12.038

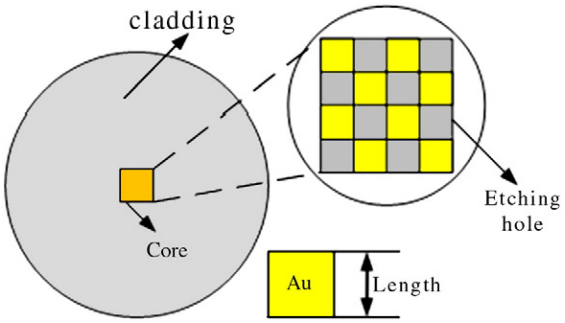

Fig. 1. Shows the GNF's distal end of the optical fiber, which has an outer diameter of 125 μm and a rectangular core with a dimension of 6 μm by 6 μm. The refractive index of the GNF cladding is 1.65, and the two glasses composing the core have indexes of 1.70 and 1.50, respectively and then the materials of 1.50 refractive index were etched to a depth of about 10 nm. There exists a 30 by 30 element array, constructed with alternative high/low index glasses inside the square core.

nanostructure fiber, we found that a rectangle was more easily etched out than a circle, meanwhile, the local electric field can be effectively excited and strongly enhanced in a rectangular structure [17], so every small unit is rectangular. Moreover, in order to reduce the influence of polarization in our structure, our structure exhibits a 30 by 30 element rectangle array, a high degree of symmetry. In the experiment, we fusion spliced the GNF and the Hp-780 fiber of which the core diameter is 6 μm (Hp-780 fiber mode field diameter is 5 ± 0.5 μm), the coupling efficiency achieved 77% in our design sizes. The two glasses composing the core have indexes of 1.70 and 1.50 respectively. The material with a refractive index of 1.7 was lead-free optical heavy flint optical glass. Small changes in major components of the mixture can change the refractive index, and they have high chemical resistance. The material with a refractive index of 1.5 was doped phosphate glass, which refractive index is proportional to the concentration of the doped. The materials of 1.50 refractive index were etched to a depth of about 10 nm. The refractive index of the GNF cladding is 1.65. After nanofabrication the fiber tip should be coated with gold. The dielectric constant of gold ε_{Au} is approximated in the visible and near-IR regions by the Drude model.

$$\varepsilon_{Au}(\omega) = \varepsilon^{\infty} - \frac{\omega_p^2}{\omega^2 + i\omega\omega_c}$$

where $\varepsilon^{\infty}=9.75$ stands for the dielectric constant at infinite angular frequency, $\omega_p=1.36\times10^{16}$ rad/s is the bulk plasma frequency, which represents the natural frequency of the oscillations of free conduction electrons, and $\omega_c=1.45\times10^{14}$ rad/s, is the damping frequency of the oscillations [18]. The planar scale (side length of each square) and the thickness of the gold layer are about 200 nm and 60 nm, respectively. We assume that there are many unit cells fabricated at the position of the core of a multimode optical fiber.

The transmission spectrum and SP resonance of the SERS grid nanostructure sensor are studied through three-dimensional FDTD electromagnetic simulations, using a spatial mesh size of 2 nm along the x and y directions, and 2 nm along the z direction. The total simulation volume is the area of a unit cell equal to 400 nm*400 nm times 1200 nm in the z direction. The incident pump light propagating in the z direction is generated by a total field/scattering field technique. Uniaxial perfectly matched layers (UPML) are used at the top and bottom of the simulation domain to completely absorb waves leaving the simulation domain in the direction of propagation. Periodic boundary conditions are used in the x–y directions. The permittivity of gold is expressed by a modified Drude model which agrees well with experimental data in the spectral region between 500 nm and 1500 nm, we pay attention to the wavelength is 780 nm. A unit cell in our grid structure has a size of about 400 nm in the transverse directions, which is smaller than wavelength, and it meets the conditions of LSPR (Localized Surface Plasmon Resonance) excitation. Thus, our light source is linearly polarized Gaussian beam.

3. Results and discussion

In the first simulation a 780 nm plane wave linearly polarized was launched in the +z direction. Near infrared excitation by a 780 nm semiconductor laser is often used in vibrational molecule spectroscopy due to its limited damage to molecules. In order to make our simulation practical, we varied the length of the grid squares to keep the plasmon resonance approximately at 780 nm. Fig. 2 gives the electromagnetic field distribution of Ex components at the distal end of the grid nanostructure fiber sensor, where the length and thickness of the grid geometry are 200 nm and 60 nm respectively. In this case, the spatial mesh sizes are 2 nm in both x and y directions. We can see that the SP can be effectively excited and strongly enhanced electric field is obtained in this sensor.

3.1. Excitation spectral

We now investigate a plasmon-wave transduction mechanism in detail. In Fig. 3, we present losses of the core-guided modes in a wavelength range of 500 nm–1500 nm for the GNF. The blue curve corresponds to Ngas = 1, and features three plasmonic excitation peaks, the maximum located at 781.3 nm. The cyan curve corresponds to Ngas = 1.1, and features three plasmonic excitation peaks, the maximum located at 800 nm. The red dotted curve corresponds to Ngas = 1.01, and also features three plasmonic excitation peaks, the maximum located at 781.2 nm. To demonstrate the potential of these fibers for sensing, we present the blue, cyan and red dotted curves, losses of the core-guided modes when the analyte refractive index is varied. As a result, positions of the plasmonic resonances shift by 18.7 nm, with the maximum peak being the most sensitive to the changes in the analyte refractive index n = 1 to 1.1(Δn = 0.1); while the analyte refractive index from n = 1 to 1.01(Δn = 0.01) changes, the plasmonic resonances shift slight only 0.1 nm. When $\Delta n=10^{-3}$ we find that the two curves are overlapped (not plotted in Fig. 3); it means the plasmonic resonance peak is invariant. While the variables of the refractive index of gas are in a magnitude of 10^{-4}, so with our sensors, the plasmonic resonance peak is invariant, and has good stability. Can keep on working under the high efficiency of enhance.

The plasmon wave, being a surface excitation, is also very sensitive to the thickness of a metallic layer. In Fig. 4, we show changes in the spectra of the plasmonic peaks for GNF when the thickness of a gold layer is varied. Generally, modal propagation loss at resonance increases when the thickness of a gold layer increases, and

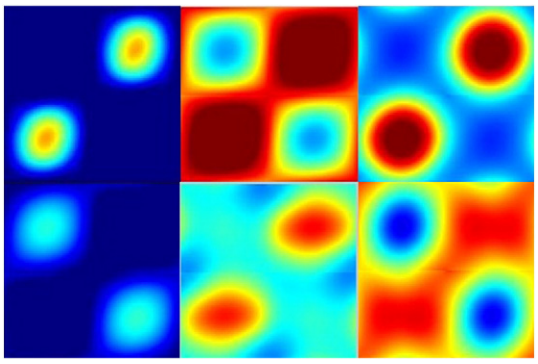

Fig. 2. Shows the time history of electromagnetic field distribution of Ex components at the distal end of the grid nanostructure fiber sensor unit, wherein the length and thickness of the grid geometry are 200 nm and 60 nm respectively. It contains six pictures.

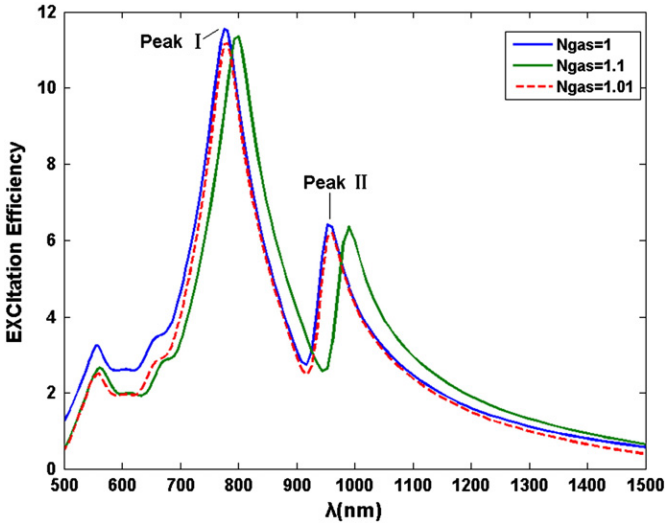

Fig. 3. Shows losses of the core-guided modes in a wavelength range of 500 nm–1500 nm for the GNF in a different environment, wherein the length and thickness of the grid geometry are 200 nm and 60 nm respectively.

simultaneously, center wavelengths of the peaks shift toward shorter wavelengths. For example, the position of a plasmonic maximum peak shifts from 800 nm to 781.3 nm when the gold layer thickness increases from 50 to 60 nm. So the LSP resonance properties of a metal nanoparticle depend on its size, shape, and the permittivity, as well as the dielectric environment. To increase the enhancement of the near field, many studies have optimized the nanoparticle geometry.

3.2. Double-resonance plasmon

According to the Figs. 3 and 4, we can see two main plasmonic maximum peaks. For example, in Fig. 3 of the blue curve, peak II corresponds to the LSP and peak I to the coupling LSP between the Au nanocubes. In addition, the simulations predicted that the extinction efficiency of coupling LSP is about twice as large as the single one. This is due to the fact that, when the array periodicity is appropriately chosen, the strong coupling between the LSP and the LSP enhances the near field intensity. Besides the large near field enhancement, the double-resonance spectrum, is another favorable feature for SERS.

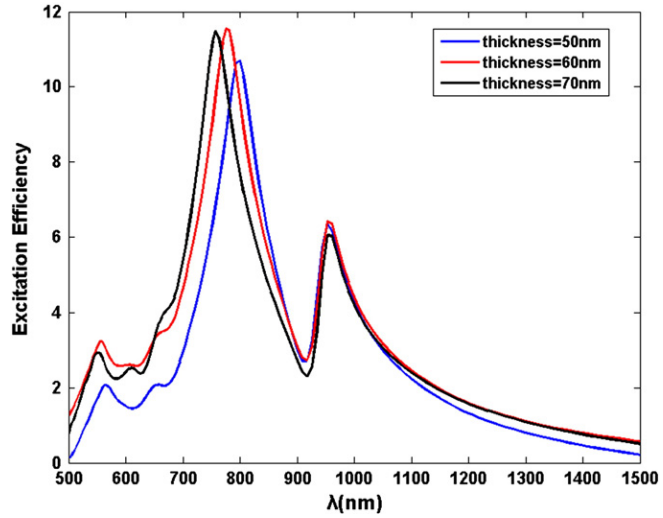

Fig. 4. Shows changes in the spectra of the plasmonic peaks for GNF when the thickness of a gold layer is varied; the length is 200 nm.

Different from single-resonance structures, the double-resonance structure, with near-field intensity peaking at two resonance frequencies, presents the opportunity for simultaneous enhancement at both the excitation and the specific Raman Stokes lines [19].

The electromagnetic enhancement factor G_{SERS} can be approximately expressed by the fourth power of the ratio of the total electric field E (r_m,υ) at the molecule location r_m to the incident excitation field $E_{inc}(\upsilon)$,

$$G_{SERS}(r_m,\nu) = \left|\frac{E(r_m,\nu)}{E_{inc}(\nu)}\right|^4$$

where υ is the laser frequency [20]. The calculations indicate that the maximum theoretical electromagnetic enhancement factor can reach almost 10^{10} in our grid nanostructure fiber sensor.

GNF is a Au nanocube array, existing strong coupling between the Au nanocubes, so it can produce double main plasmon peak, but a single Au nanocube cannot. In order to understand the physics behind the coupling effects, Fig. 5 demonstrates the E-field amplitude (E_x) patterns for an Au cube at horizontal direction polarizations, (A) shows the field distribution of cube dimer, and (B) shows the field distribution of a single cube. The black line represents the Au nanocube frame, (A) and (B) in the same conditions. When the electric field is polarized parallel to the dimer axis, the maximum of the near-field enhancements is focused between the nanocubes. The plasmon modes of each of the nanocube are aligned, inducing a large electric field across the junction. In (A), we show strong coupling field, while in (B), electric field is very weak. The figure clearly shows that the electric field coupling is strong at the dimer.

3.3. Polarization effects

Finally, we study the polarization effect. Previous investigations of polarization effects on nanorods and nanocubes [17,21] indicated that the polarization of the incident light plays an important role in the SERS process. Therefore, to optimize the electromagnetic enhancement factor, one must take into account the vectorial nature of the fields involved. The structure we design is symmetrical, so the local field enhancement will repeat every 45°. According to ref. [12], we know that with the change of the polarization angle, the wavelength of motion is monotonous. So we only need to take into account the polarizations from 0° to 45°. In Table 1, the biggest change of the polarization angle for wavelength is $|\Delta\lambda_{max}| = 6.7$ nm for Peak I and $|\Delta\lambda'_{max}| = 8.4$ nm for Peak II, so wavelengths shift caused by the polarization $|\Delta\lambda| \leq 8.4$ nm. Compared with ref. [22], the polarization effect on the resonance wavelength can be negligible. Therefore, we don't need to worry about the shift of the resonance wavelength when we adjust the polarization of the incident light to obtain the maximum electromagnetic enhancement factor.

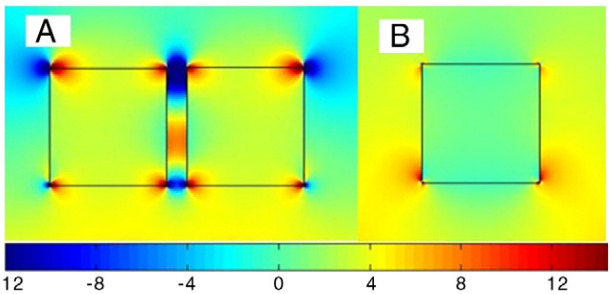

Fig. 5. Demonstrates the E-field amplitude (Ex) patterns for an Au cube at horizontal direction polarizations, (A) shows the field distribution of a cube dimer, (B) shows the field distribution of a single cube. The black line represents the Au nanocube frame, (A) and (B) in the same conditions.

Table 1
The resonance wavelength differences of the extinction spectra for different polarizations.

Polarization angle	λmax (nm)	
	Peak I	Peak II
$\theta_1 = 0°$	788.0	944.0
$\theta_2 = 45°$	781.3	952.4

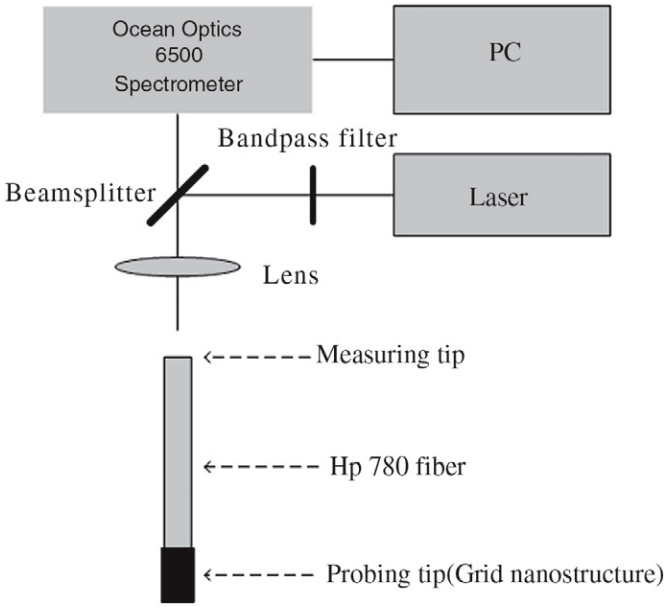

Fig. 6. A schematic diagram of the experiment setup.

3.4. Applications of the grid nanostructure device for SERS

Our typical experiment setup can be designed as shown in Fig. 6: a microscope objective lens is used to couple the excitation laser into the fiber (Hp-780, about 10 to 15 cm).Owing to the big loss of the grid nanostructure fiber, the length is less than 100 um. In the experiment, we use the 70 um long GNF, and the backscattering SERS signal is also collected by the objective lens into the Ocean Optics Raman spectrometer. The coupling between the objective lens and the fiber is carefully calibrated to eliminate the loss as much as possible. A laser (780 nm) is used as an excitation source to verify the broad spectral characteristic of the SERS probe.

4. Conclusion

We have introduced a novel grid nanostructure design that can be used as an effective SERS fiber sensor when fabricated directly on the tip of an optical fiber. With our structure, the plasmonic resonance peak has a good stability and keeps on working under the high efficiency of enhance. Double-resonance plasmon can be effectively excited, which is more than 2 orders of magnitude larger than the single resonance plasmon under the same conditions. So strong local field enhancement can be obtained. Our studies also showed the dependence on structural parameters and can be used to optimize the nanostructure geometry. Moreover, the structure we designed is symmetric, so the polarization effect on the resonance wavelength can be negligible.

Acknowledgment

This work was supported by a grant (Nos. 60807017 and 60937002) from the Natural Science Foundation of China.

References

[1] N. Guillot, H. Shen, B. Frémaux, O. Péron, E. Rinnert, T. Toury, M. Lamy dela Chapelle, Appl. Phys. Lett. 97 (2010) 023113.
[2] Jixin Yanga, Adrian Amezcua-Correab, Anna C. Peacockb, Chris E. Finlaysonb, Jeremy J. Baumbergc, Steven M. Howdlea, Pier J.A. Saziob, Proc. SPIE 6369 (2006) 636906.
[3] Davidl Stokes, Zhenhuan Chi, Vo-Dinh Tuan, Appl. Spectrosc. 58 (2004) 292.
[4] M. Kahl, E. Voges, S. Kostrewa, C. Viets, W. Hill, Sens. Actuators B 51 (1998) 285.
[5] E. Perevedentseva, A. Karmenyan, P.-H. Chung, C.-L. Cheng, J. Vac. Sci. Technol. B 23 (2005) 1980.
[6] A. Lucotti, G. Zerbi, Sens. Actuators B 121 (2007) 356.
[7] A. Lucotti, A. Pesapane, G. Zerbi, Appl. Spectrosc. 61 (2007) 260.
[8] Y. Zhang, C. Gu, A.M. Schwartzberg, J.Z. Zhang, Appl. Phys. Lett. 87 (2005) 123105.
[9] H.Y. Chu, Y. Liu, Y. Huang, Y. Zhao, Opt. Express 15 (2007) 12230.
[10] C. Gu, Y. Zhang, A.M. Schwartzberg, J.Z. Zhang, Proc. SPIE 5911 (2005) 591108.
[11] D.L. Stokes, Z.H. Chi, T. Vo-Dinh, Appl. Spectrosc. 58 (2004) 292.
[12] Shuqi Chen, Lin Han, Axel Schülzgen, Hongbo Li, Li. Li, Jerome V. Moloney, N. Peyghambarian, Opt. Express 16 (2008) 13016.
[13] A. Dhawan, J.F. Muth, Nanotechnology 17 (2006) 2504.
[14] A. Dhawana, Y. Zhang, F. Yan, M. Gerholda, T. Vo-Dinh, Proc. SPIE 6869 (2008) 68690.
[15] D.J. White, P.R. Stoddart, Opt. Lett. 30 (2005) 598.
[16] William L. Barnes, Alain Dereux, Thomas W. Ebbesen, Nature 424 (2003) 824.
[17] J.M. McLellan, Z.Y. Li, A.R. Siekkinen, Y. Xia, Nano Lett. 7 (2007) 1013.
[18] Alireza Hassani, Maksim Skorobogatiy, Opt. Soc. Am. B 24 (2007) 1423.
[19] Chu Yizhuo, Mohamad G. Banaee, Kenneth B. Crozier, Acs Nano 4 (5) (2010) 2804.
[20] F.J. García-Vidal, J.B. Pendry, Phys. Rev. Lett. 77 (1996) 1163.
[21] Y. Liu, J. Fan, Y.P. Zhao, S. Shanmukh, R.A. Dluhy, Appl. Phys. Lett. 89 (2006) 173134.
[22] N. Félidj, J. Aubard, G. Le, Appl. Phys. Lett. 82 (2003) 3095.